Application of Cloude's target decomposition theorem to polarimetric imaging radar data

Jakob J. van Zyl

Jet Propulsion Laboratory
California Institute of Technology
4800 Oak Grove Drive, Pasadena, CA 91109

ABSTRACT

In this paper we applied Cloude's decomposition to imaging radar polarimetry. We show in detail how the decomposition results can guide the interpretation of scattering from vegetated areas. For multifrequency polarimetric radar measurements of a clear-cut area, the decomposition leads us to conclude that the vegetation is probably thin compared to even the C-band radar wavelength of 6 cm. For a forested area, we notice an increased amount of even number of reflection scattering at P-band and L-band, probably the result of penetration through the coniferous canopy resulting in trunk-ground double reflection scattering. The scattering for the forested area is still dominated by scattering from randomly oriented cylinders, however. It is found that these cylinders are thicker than in the case of clear-cut areas, leading us to conclude that scattering from the branches probably dominates in this case.

1. INTRODUCTION

In the analysis of polarimetric imaging radar data, one is often faced with the situation where some geophysical parameters must be inferred from an area that exhibits significant natural variability in the scattering properties. In such cases, the resulting average Stokes or covariance matrix differs significantly from that of a single scatterer. It has long been speculated that if a unique way could be found to decompose such an average Stokes or covariance matrix into a sum of matrices representing single scatterers, one would not only be able to more accurately interpret the scattering processes, but the problem of inferring geophysical parameters from the measured radar data would also be significantly simplified.

One of the first examples of such a target decomposition technique was provided by Chandrasekhar [1] in his book on radiative transfer. Considering the case of lateral scattering of light by small anisotropic particles, he decomposed the total average phase matrix into the sum of a phase matrix that represents dipole scattering and a phase matrix that represents pure random scattering, or noise. As such, his target decomposition followed the same principle that breaks the Stokes vector of a partially polarized wave into the sum of a Stokes vector representing a fully polarized wave, and a Stokes vector representing a completely unpolarized wave (see Papas [2] for example).

Huynen [3], in his thesis published in 1970, also introduced a target decomposition theorem in which he decomposed an average Mueller matrix into the sum of a Mueller matrix for single a scatterer and a "noise" or N-target Mueller matrix. However, unlike Chandrasekhar's decomposition, Huynen's N-target is not polarization independent, and has been shown to be just one of an infinite set of such residue matrices, meaning that Huynen's decomposition is not unique.

In 1988 Cloude [4] introduced a target decomposition based on an eigenvector decomposition of the target covariance matrix. This decomposition was shown to be unique and, in the monostatic case, breaks the average covariance matrix up into the weighted sum of three covariance matrices representing three different single scatterers, analogous to the decomposition of a Stokes vector of a partially polarized wave into the sum of the Stokes vectors of two full polarized waves that are orthogonally polarized [2].

In this paper we examine the application of Cloude's decomposition to the analysis of polarimetric synthetic aperture radar (SAR) data.

2. CLOUDE'S DECOMPOSITION

Cloude showed that a general covariance matrix **[T]** can be decomposed as follows:

$$[\mathbf{T}] = \sum_{i=1}^{4} \lambda_i \quad \mathbf{k}_i \cdot \mathbf{k}_i^{\dagger} \tag{1}$$

In (1), $\lambda_i \; ; i = 1,2,3,4$ are the eigenvalues of the covariance matrix, $\mathbf{k}_i \; ; i = 1,2,3,4$ are the eigenvectors of **[T]**, and $\mathbf{k}_i^{\dagger}$ means the *adjoint* (complex conjugate transposed) of $\mathbf{k}_i$. In the monostatic case, for reciprocal media, the covariance matrix has one zero eigenvalue and the decomposition results in at most three covariance matrices on the right-hand side of (1).

In (1) the elements of the eigenvectors are the elements of an equivalent scattering matrix in the basis in which the decomposition is performed. For example, if the covariance matrix elements are expressed in the normal HV basis, then the four elements of the eigenvectors are simply the four scattering matrix elements in the linear basis. Also, since the covariance matrix is, by definition, a hermitian matrix, it follows that the eigenvalues are all real, and the eigenvectors are orthogonal. Therefore, one can interpret (1) to mean that this decomposition breaks the covariance matrix into the weighted sum of covariance matrices from "orthogonal" scattering matrices.

Cloude did his decomposition in the basis formed by the Pauli spin matrices, but pointed out that the decomposition can be done using any four complex matrices that satisfy the constraint of completeness and normalization. Here, we shall interpret our results in the natural linear basis in which the radar measurements are performed.

Also useful in our discussions later is Cloude's definition of target entropy,

$$H_T = -\sum_{i=1}^{4} P_i \log_4 P_i \tag{2}$$

where

$$P_i = \frac{\lambda_i}{\lambda_1 + \lambda_2 + \lambda_3 + \lambda_4} \tag{3}$$

As pointed out by Cloude, the target entropy is a measure of target disorder, with $H_T = 1$ for random targets and $H_T = 0$ for simple (single) targets.

3. DECOMPOSITION OF SCATTERING FROM AZIMUTHALLY SYMMETRIC NATURAL TERRAIN

Before getting into the radar data analysis, let us illustrate the decomposition using a general description of the covariance matrix for azimuthally symmetrical natural terrain in the monostatic case. Borgeaud *et al.* [5] showed using a random medium model, that the average covariance matrix for azimuthally symmetrical terrain in the monostatic case has the general form

$$[\mathbf{T}] = C\begin{pmatrix} 1 & 0 & \rho \\ 0 & \eta & 0 \\ \rho^* & 0 & \zeta \end{pmatrix} \tag{4}$$

where

$$C = \langle S_{hh} S_{hh}^* \rangle \tag{5}$$

$$\rho = \frac{\langle S_{hh} S_{vv}^* \rangle}{\langle S_{hh} S_{hh}^* \rangle} \tag{6}$$

$$\eta = 2\frac{\langle S_{hv} S_{hv}^* \rangle}{\langle S_{hh} S_{hh}^* \rangle} \tag{7}$$

$$\zeta = \frac{\langle S_{vv} S_{vv}^* \rangle}{\langle S_{hh} S_{hh}^* \rangle} \tag{8}$$

The superscript * means complex conjugate, and all quantities are ensemble averages. The parameters C, η, ζ and ρ all depend on the size, shape and electrical properties of the scatterers, as well as their statistical angular distribution. It is easily shown that the eigenvalues of **[T]** are

$$\lambda_1 = \frac{C}{2}\left\{\zeta + 1 + \sqrt{(\zeta-1)^2 + 4|\rho|^2}\right\} \tag{9}$$

$$\lambda_2 = \frac{C}{2}\left\{\zeta + 1 - \sqrt{(\zeta-1)^2 + 4|\rho|^2}\right\} \tag{10}$$

$$\lambda_3 = C\,\eta \tag{11}$$

The corresponding three eigenvectors are

$$\mathbf{k}_1 = \sqrt{\frac{\left[\zeta - 1 + \sqrt{\Delta}\right]^2}{\left[\zeta - 1 + \sqrt{\Delta}\right]^2 + 4|\rho|^2}} \begin{pmatrix} 2\rho \,/\, \left[\zeta - 1 + \sqrt{\Delta}\right] \\ 0 \\ 1 \end{pmatrix} \tag{12}$$

$$\mathbf{k}_2 = \sqrt{\frac{\left[\zeta - 1 - \sqrt{\Delta}\right]^2}{\left[\zeta - 1 - \sqrt{\Delta}\right]^2 + 4|\rho|^2}} \begin{pmatrix} 2\rho \,/\, \left[\zeta - 1 - \sqrt{\Delta}\right] \\ 0 \\ 1 \end{pmatrix} \tag{13}$$

$$\mathbf{k}_3 = \begin{pmatrix} 0 \\ 1 \\ 0 \end{pmatrix} \tag{14}$$

In these expressions, we used the shorthand notation

$$\Delta = [\zeta - 1]^2 + 4|\rho|^2 \tag{15}$$

We note that Δ is always positive. Also note that we can write the ratio of the first elements of the first two eigenvectors as

$$\frac{k_{11}}{k_{21}} = -\sqrt{\frac{\left[\zeta - 1 + \sqrt{\Delta}\right]^2\left(\left[\zeta - 1 - \sqrt{\Delta}\right]^2 + 4|\rho|^2\right)}{\left[\zeta - 1 - \sqrt{\Delta}\right]^2\left(\left[\zeta - 1 + \sqrt{\Delta}\right]^2 + 4|\rho|^2\right)}}\ \frac{\left[\zeta - 1 - \sqrt{\Delta}\right]^2}{4|\rho|^2} \tag{16}$$

which is always negative. This means that the first two eigenvectors represent scattering matrices that can be interpreted in terms of odd and even numbers of reflections. In the rest of this paper, we shall examine decompositions of the form shown above for different types of terrain using measured polarimetric radar data.

4. EXAMPLES OF CLOUDE DECOMPOSITION}

4.1 Randomly oriented dielectric cylinders.

Before analyzing measured data, let us examine a special theoretical case of uniformly randomly oriented dielectric cylinders. In general, the scattering matrix of a single dielectric cylinder oriented horizontally can be written as

$$[\mathbf{S}] = \begin{pmatrix} a & 0 \\ 0 & b \end{pmatrix} \tag{17}$$

where a and b are complex numbers whose magnitudes and phases are functions of cylinder dielectric constant, diameter and length [6]. Generally, when the cylinder is thin compared to the wavelength, $|a| > |b|$. To calculate the average covariance matrix for randomly oriented cylinders, one has to apply a rotation operator to **[S]** and average the results over all angles of orientation. Assuming a uniform distribution in angles about the line of sight, one can easily show that the resulting average covariance matrix for the monostatic case is of the form given in (4) with

$$C = \left[3|a|^2 + 3|b|^2 + 2\Re\left(a^* b\right)\right] / 8 \tag{18}$$

$$\rho = \frac{\left[|a|^2 + |b|^2 + 6\Re\left(a^* b\right)\right]}{\left[3|a|^2 + 3|b|^2 + 2\Re\left(a^* b\right)\right]} \tag{19}$$

$$\eta = \frac{2|a-b|^2}{\left[3|a|^2 + 3|b|^2 + 2\Re\left(a^* b\right)\right]} \tag{20}$$

$$\zeta = 1 \tag{21}$$

It is easily shown using (9) -- (14) that

$$\lambda_1 = C(1+|\rho|) \tag{22}$$

$$\lambda_2 = C(1-|\rho|) \tag{23}$$

$$\lambda_3 = C\,\eta \tag{24}$$

The corresponding three eigenvectors are

$$\mathbf{k}_1 = \frac{1}{\sqrt{2}} \begin{pmatrix} \rho / |\rho| \\ 0 \\ 1 \end{pmatrix} \tag{25}$$

$$\mathbf{k}_2 = \frac{1}{\sqrt{2}}\begin{pmatrix} -\rho/|\rho| \\ 0 \\ 1 \end{pmatrix} \tag{26}$$

$$\mathbf{k}_3 = \begin{pmatrix} 0 \\ 1 \\ 0 \end{pmatrix} \tag{27}$$

From (19) and (20), it is easily shown that

$$1 - |\rho| = \eta \tag{28}$$

This means that for the case of randomly oriented cylinders, the second and third eigenvalues are the same.

In the thin cylinder limit, $|b|$ approaches zero, and we find that

$$\rho_{thin} = 1/3 \tag{29}$$

$$\eta_{thin} = 2/3 \tag{30}$$

$$[\mathbf{T}] = C\left\{\frac{2}{3}\begin{pmatrix} 1 & 0 & 1 \\ 0 & 0 & 0 \\ 1 & 0 & 1 \end{pmatrix} + \frac{1}{3}\begin{pmatrix} 1 & 0 & -1 \\ 0 & 0 & 0 \\ -1 & 0 & 1 \end{pmatrix} + \frac{2}{3}\begin{pmatrix} 0 & 0 & 0 \\ 0 & 1 & 0 \\ 0 & 0 & 0 \end{pmatrix}\right\} \tag{31}$$

In this case, equal amounts of scattering are contributed by the matrix that resembles scattering by a sphere (or a trihedral corner reflector) and by the cross-polarized return, although a significant fraction of the total energy is also contained in the third matrix resembling scattering by a dihedral corner reflector. The entropy in this case is 0.95 indicating a high degree of target disorder or randomness.

On the other hand, in the thick cylinder limit, $|b|$ approaches $|a|$ and we find that

$$\rho_{thick} = 1 \tag{32}$$

$$\eta_{thick} = 0 \tag{33}$$

In this case, only one eigenvalue is non-zero, and the average covariance matrix is identical to that of a sphere (pr a trihedral corner reflector). The entropy is 0, indicating no target randomness, even though we have calculated the average covariance matrix for *randomly oriented* thick cylinders! The explanation for this result lies in the fact that when the cylinders are thick, the single cylinder scattering matrix becomes the identity matrix, which is insensitive to rotations. Therefore, even after rotations, we still added up only identity matrices, and no apparent target randomness is introduced.

For cylinders that are neither thick compared to the wavelength, nor thin compared to the wavelength, $0 \leq |b/a| \leq 1$. Figure 1 shows the behavior of the normalized the eigenvalues as predicted by (22)-(24). We notice, as mentioned before, that the

second and third eigenvalues are always the same magnitude, but they get smaller relative to the first eigenvalue as the ratio of the two scattering matrix elements approaches 1.

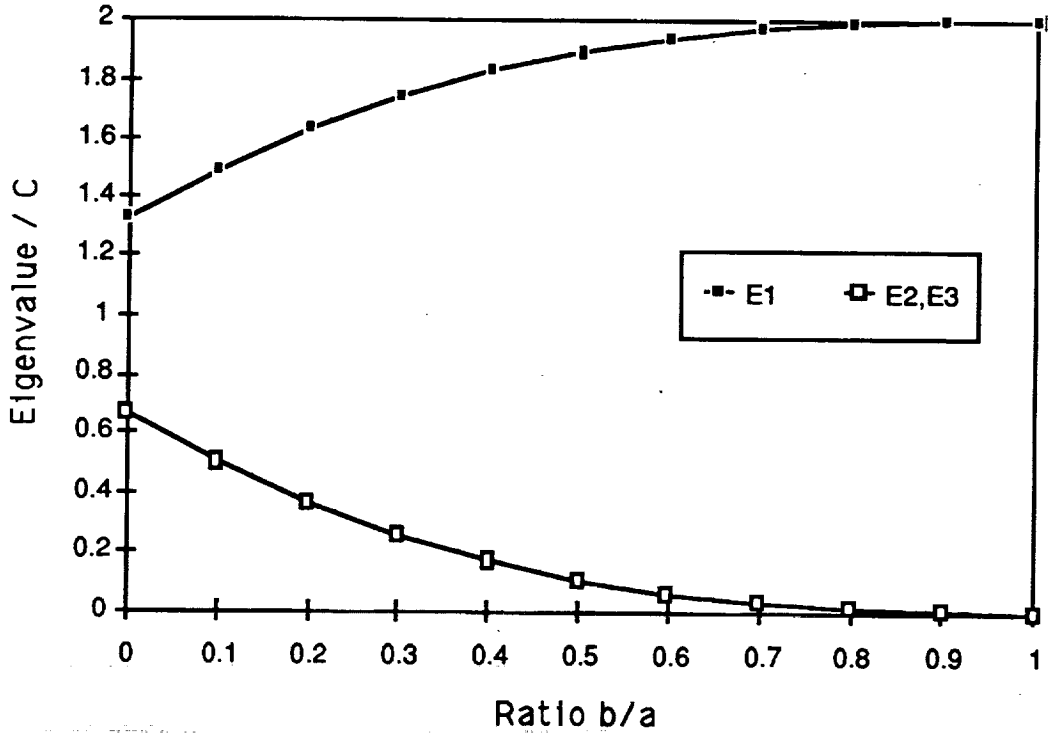

Figure 1. *Ratio of eigenvalues as a function of the ratio of b to a. The ratio of b to a depends on the cylinder dielectric constant and cylinder size compared to the wavelength.*

4.2 Measured scattering from clear-cut area.

Using the NASA/JPL AIRSAR system [7], the complete Stokes matrix [8] can be measured for each pixel in a scene. The actual measurements in general compare well with the general form of the covariance matrix assumed in (8), except that the four terms assumed to be zero are not exactly equal to zero. However, these four terms are typically much smaller than the other terms, so that to a good approximation, the assumption in (8) is valid. Here, we shall set those four terms to zero. Table 1 below shows the measured parameters at P-band, L-band and C-band for a clear-cut area in the Shasta Trinity National Forest in California.

The clear-cut area is covered with short shrub-like vegetation. We note that at all three frequencies the scattering is dominated by an odd number of reflections. At P-band the

even number of reflections and the cross-polarized returns are almost the same strength, and about half that of the odd numbers of reflections. This is very similar to the thin randomly oriented cylinder case discussed earlier. As the frequency increases, the even number of reflections and the cross-polarized returns become more different, and also become a smaller fraction of the total scattering. This is consistent with the randomly oriented cylinder case where the radius of the cylinder increases. The same conclusion is reached when considering the entropy. The highest value (most randomness) is observed at P-band, and the randomness decreases with increasing frequency. As pointed out before, as the cylinder radius increases, the entropy decreases. Therefore, from the decomposition results we conclude that the vegetation in the clear-cut is randomly oriented, and that most of the scattering comes from vegetation that has branches that are thin compared to the three radar wavelengths.

Table 1. *Measured values for a clear-cut in the Shasta Trinity National Forest. Also shown are the results of the Cloude decomposition.*

Parameter	P-band	L-band	C-band
η	0.5261	0.5308	0.4083
ζ	0.5642	0.7580	0.7159
ρ	0.0928+i0.0582	0.2324+i0.1057	0.3558+i0.0440
λ_1	1.0260	1.1615	1.2437
λ_2	0.5382	0.5964	0.4722
λ_3	0.5261	0.5308	0.4083
Entropy	0.95	0.94	0.88

4.3 Measured scattering from a forested area.

Table 2 below shows the measured parameters at P-band, L-band and C-band for a forested area in the Shasta Trinity National Forest in California. We note that at all three frequencies the scattering from this coniferous forest is dominated by an odd number of reflections. At P-band the even number of reflections contribution is stronger relative to the cross-polarized returns when compared to the case of scattering by randomly oriented cylinders. This is likely a result of the P-band signals penetrating through the canopy and then suffering a double reflection when scattering from the ground and then from the tree trunks before returning to the radar. We notice that the imbalance of the even numbers of reflections and the cross-polarized returns decrease as the frequency increases, and also become a smaller fraction of the total scattering. A possible interpretation of this is that as the frequency increases, the penetration

through the canopy decreases and the scattering from the randomly oriented branches becomes more important. The highest value of the entropy (most randomness) is

Table 2. *Measured values for a forested area in the Shasta Trinity National Forest. Also shown are the results of the Cloude decomposition.*

Parameter	P-band	L-band	C-band
η	0.3301	0.3485	0.2416
ζ	0.6529	0.7122	0.4685
ρ	0.2803+i0.0167	0.3950+i0.0582	0.3669+i0.0016
λ_1	1.1566	1.2805	1.1873
λ_2	0.4963	0.4316	0.2812
λ_3	0.3301	0.3485	0.2416
Entropy	0.87	0.84	0.75

observed at P-band, and the randomness decreases with increasing frequency. From the decomposition results we conclude that the penetration through this coniferous canopy cannot be neglected. Most of the scattering can still be contributed to the randomly oriented branches, however. The relative strengths of the different mechanisms, as well as the lower values of the entropy, suggest that the branches are thicker than those of the vegetation in the clear-cut area.

5. DISCUSSION

In this paper we applied Cloude's decomposition to imaging radar polarimetry. The decompositions illustrated here have been implemented on a pixel-by-pixel basis to analyze polarimetric radar images. Space does not permit the inclusion of more examples, however.

We have shown how the decomposition results can guide the interpretation of scattering from vegetated areas. For clear-cut areas, we concluded that the vegetation is probably thin compared to even the C-band radar wavelength of 6 cm. For forested areas, we noticed an increased amount of even number of reflection scattering at P-band and L-band, probably the result of penetration through the coniferous canopy resulting in trunk-ground double reflection scattering. The scattering for the forested area is still dominated by scattering from randomly oriented cylinders. It is found that these cylinders are thicker than in the case of clear-cut areas, leading us to conclude that scattering from the branches probably dominates in this case.

The quantitative analysis of scattering requires detailed analysis of the decompositions that will result from model predictions. Future work will concentrate on analyzing the decompositions of model predicted covariance matrices. The results can then be used to analyze polarimetric radar images.

6. ACKNOWLEDGMENT

This work was performed at the Jet Propulsion Laboratory, California Institute of Technology with a grant from the Director's Discretionary Fund.

7. REFERENCES

[1] S. Chandrasekhar, *Radiative Transfer*, Dover Publications, New York, p. 50, 1960.

[2] C. H. Papas, *Theory of Electromagnetic Wave Propagation*, Dover Publications, New York, pp. 118-134, 1988.

[3] J. R. Huynen, *Phenomenological Theory of Radar Targets*, Ph.D. dissertation, Drukkerij Bronder-Offset, N.V., Rotterdam, Netherlands, 1970.

[4] S. R. Cloude, "Uniqueness of target decomposition theorems in radar polarimetry," *Direct and Inverse Methods in Radar Polarimetry: Part 1*, W.M. Boerner (Ed.), Kluwer Academic Publishers, Dordrecht, Germany, pp. 267-296, 1992.

[5] M. Borgeaud, R. T. Shin and J. A. Kong, "Theoretical models for polarimetric radar clutter," *Journal of EM Waves and Applications*, 1, pp. 73-91, 1987.

[6] C. F. Bohren and D. R. Huffman, *Absorption and Scattering of Light by Small Particles*, Wiley and Sons, New York, 1983.

[7] J. van Zyl, R. Carande, Y. Lou, T. Miller, and K. Wheeler, "The NASA/JPL three-frequency polarimetric AIRSAR system," *Proceedings of IGARSS'92*, Volume I, pp. 649-651, 1992.

[8] J. J. van Zyl, H.A. Zebker and C. Elachi, "Imaging radar polarization signatures: Theory and observation," *Radio Science*, 22, pp. 529-543 , 1987.